

Structure and Functional Characterization of the Conserved JAK Interaction Region in the Intrinsically Disordered N-Terminus of SOCS5

Indu R. Chandrashekar,^{*,†} Biswaranjan Mohanty,[†] Edmond M. Linossi,^{‡,§} Laura F. Dagley,^{‡,§} Eleanor W. W. Leung,[†] James M. Murphy,^{‡,§} Jeffrey J. Babon,^{‡,§} Sandra E. Nicholson,^{‡,§} and Raymond S. Norton^{*,†}

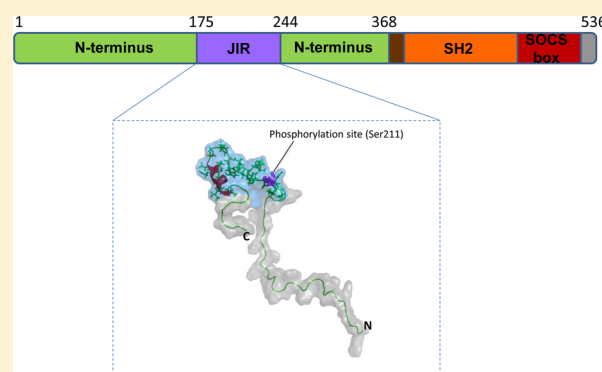
[†]Medicinal Chemistry, Monash Institute of Pharmaceutical Sciences, Monash University, 381 Royal Parade, Parkville, Victoria 3052, Australia

[‡]The Walter & Eliza Hall Institute of Medical Research, 1G Royal Parade, Parkville, Victoria 3052, Australia

[§]The Department of Medical Biology, University of Melbourne, Parkville, Victoria 3052, Australia

S Supporting Information

ABSTRACT: SOCS5 can negatively regulate both JAK/STAT and EGF-receptor pathways and has therefore been implicated in regulating both the immune response and tumorigenesis. Understanding the molecular basis for SOCS5 activity may reveal novel ways to target key components of these signaling pathways. The N-terminal region of SOCS5 coordinates critical protein interactions involved in inhibition of JAK/STAT signaling, and a conserved region within the N-terminus of SOCS5 mediates direct binding to the JAK kinase domain. Here we have characterized the solution conformation of this conserved JAK interaction region (JIR) within the largely disordered N-terminus of SOCS5. Using nuclear magnetic resonance (NMR) chemical shift analysis, relaxation measurements, and NOE analysis, we demonstrate the presence of preformed structural elements in the JIR of mouse SOCS5 (mSOCS5_{175–244}), consisting of an α -helix encompassing residues 224–233, preceded by a turn and an extended structure. We have identified a phosphorylation site (Ser211) within the JIR of mSOCS5 and have investigated the role of phosphorylation in modulating JAK binding using site-directed mutagenesis.



The suppressor of cytokine signaling (SOCS) proteins are small intracellular proteins that negatively regulate cytokine responses by binding to receptor complexes and inhibiting the activity of the associated JAK tyrosine kinases, or by targeting signaling components for ubiquitination and proteasomal degradation.^{1–3} The mammalian SOCS family consists of eight proteins, SOCS1–7 and cytokine-inducible SH2-containing protein (CIS), that share a common domain organization, with a central SH2 domain, a highly conserved C-terminal SOCS box, and an N-terminal region of low sequence conservation.^{4,5} The N-terminal domains of SOCS proteins vary in sequence and length, with SOCS4–7 being distinguished from the other SOCS proteins by long N-terminal regions, which are predicted to be disordered.⁶ In general, SOCS proteins are thought to bind to target proteins via their SH2 domains or N-terminal regions, leading to ubiquitination of the target protein by the SOCS box-associated E3 ubiquitin ligase complex and its subsequent proteasomal degradation.^{7,8}

While the physiological functions of SOCS1–3 and CIS are well characterized,^{2,5,9} comparatively little is known regarding

the biological roles of SOCS4 and SOCS5. Although SOCS4 and SOCS5 share high sequence homology across their SH2 domain (~90%) and SOCS box, it is unclear whether they have overlapping or distinct biological roles.^{5,8,10,11} However, SOCS5 can interact independently of the canonical SH2-phosphotyrosine interactions via its N-terminus, which mediates interactions with the EGF receptor^{8,10} and IL-4 receptor.¹² Recently, SOCS36E, the SOCS5 homologue in *Drosophila*, was shown to negatively regulate JAK/STAT signaling via a SOCS box-independent interaction mediated by the N-terminus.¹³ Studies in *Drosophila* suggest that the EGF receptor and JAK/STAT pathways cooperate in oncogenic transformation and are both able to induce the expression of SOCS36E, which, in turn, serves to limit the activity of both pathways.¹⁴ There is also increasing evidence that mammalian SOCS5 may function as a tumor suppressor.

Received: June 4, 2015

Revised: July 13, 2015

Published: July 14, 2015

sor.^{15,16} Recently, SOCS5 was identified as a target of microRNA (miR) miR-9, down-regulation of SOCS5 expression by which resulted in aberrant activation of JAK/STAT signaling in tumor-associated endothelial cells.¹⁷ These findings highlight the potential role of SOCS5 in the regulation of oncogenic signaling, although the molecular mechanisms by which it acts in these pathways have not been well-defined. Understanding these events may provide a rationale for targeting these pathways through the development of novel cancer therapeutics that mimic or block the activity of SOCS5.

In contrast to the relative wealth of structural and functional data available for the SH2 domain and the SOCS box,^{7,18–21} little is known about the structure and function of the N-terminal region of the SOCS proteins. In most studies the N-terminal regions of SOCS proteins were removed to avoid interference with structure determination. However, we recently identified a highly conserved 70-residue region in the disordered N-terminus of SOCS4 and SOCS5 that is predicted to be more ordered than the surrounding sequence.⁶ The high degree of sequence conservation of this region across species and extending back to lower vertebrates implies that it has an important functional role.⁶ We also demonstrated that SOCS5 could bind all four JAK family members, although it was found to selectively inhibit only JAK1 and JAK2 autophosphorylation, and this function was dependent on the SOCS5 N-terminal region.²² The conserved N-terminal region in SOCS5 (SOCS5_{175–244}) facilitates a direct interaction with the kinase domain of JAK and has therefore been designated the JAK interaction region (JIR).²² The equilibrium dissociation constant (K_D) for the interaction of SOCS5 JIR with the kinase domain of JAK1 was found to be 0.5 μ M.²² Deletion of the JIR impaired the ability of SOCS5 to inhibit IL-4 induced STAT6 activity, suggesting that this region was functionally important.²²

In this study, we characterize the conformation and dynamics of the JIR of mouse SOCS5 (mSOCS5_{175–244}) by solution NMR spectroscopy. We show that residues 224–233 in the C-terminal region of mSOCS5 JIR adopt a helical structure and exhibit partially restricted dynamics, while the N-terminal region is disordered and flexible. We identify a phosphorylation site within the conserved JIR of mSOCS5 and use site-directed mutagenesis and surface plasmon resonance (SPR) to probe the role of phosphorylation in modulating JAK binding.

■ EXPERIMENTAL PROCEDURES

Protein Expression and Purification. The expression and purification of mSOCS5_{175–244} were as described previously.²² The protein purity was determined to be >95% by analytical HPLC and SDS-PAGE and the molecular mass confirmed by mass spectrometry (8101 Da). [U-¹³C, ¹⁵N]-mSOCS5_{175–244} was expressed in 1 L of M9 medium supplemented with 1 g/L of ¹⁵NH₄Cl and 2 g/L of ¹³C-glucose. Expression and purification conditions were as described for unlabeled mSOCS5_{175–244}.²² The protein yields per liter of culture were generally 1–2 mg for [U-¹³C, ¹⁵N]-mSOCS5_{175–244} and 3 mg for [U-¹⁵N]-mSOCS5_{175–244}. Ser211Glu and Ser211Ala mutants of mSOCS5_{175–244} were generated using site-directed mutagenesis. Expression and purification conditions for these mutants were as described for mSOCS5_{175–244}.²²

Codon-optimized DNA corresponding to residues 110–313 in the N-terminus of mouse SOCS5 was custom synthesized (Genscript). EcoRI and TEV sites were engineered upstream of mSOCS5_{110–313} gene and a BamHI site was incorporated

downstream. This gene was ligated into the pGEX-2T vector (GE Healthcare) via EcoRI and BamHI sites and transformed into *E. coli* BL21-(DE3) cells. mSOCS5_{110–313} was expressed as a glutathione S-transferase (GST)-fusion protein. The cells were grown at 28 °C in 1 L of Luria–Bertani medium to an OD₆₀₀ 0.5, cooled to 18 °C, and protein expression was induced with 1 mM isopropyl β -D-1-thiogalactopyranoside for 20 h at 18 °C. The soluble GST-fusion protein was purified using glutathione-Sepharose 4B (GE Healthcare). One unit of TEV protease per 30 mg of fusion protein was used to cleave at 4 °C for 20 h on a rotating mixer. mSOCS5_{110–313} was further purified from the cleavage mixture using cation-exchange chromatography. Recombinant JAK kinase domains were expressed in insect cells and purified as described previously.¹⁹

NMR Spectroscopy and Resonance Assignments. Lyophilized [U-¹³C, ¹⁵N]-mSOCS5_{175–244} was dissolved in a buffer containing 20 mM sodium citrate (pH 4.5), 5 mM TCEP, 0.02% (w/v) sodium azide (NaN₃), 94% H₂O, and 6% ²H₂O, at a final protein concentration of 0.3 mM. NMR data were acquired on 600 and 800 MHz Bruker Avance spectrometers, both equipped with cryogenically cooled triple-resonance probes. Sequence-specific resonance assignments (¹H, N, C α and C β) were obtained at 30 °C using the following three-dimensional experiments, employing nonuniform sampling in the ¹⁵N and ¹³C dimensions: HNCA, CBCA(CO)NH, HNCACB. The data sets were processed with the multidimensional decomposition algorithm²³ using TOPSPIN (version 3.2) from Bruker BioSpin or NMRPipe.²⁴ Spectra were referenced to dioxane at 3.75 ppm. Data analysis and peak-picking were done using CARA and NMRView²⁵ and automated backbone assignments were made using the software MATCH in the UNIO software package.²⁶ The backbone assignments were then manually complemented and completed interactively using 3D ¹⁵N-resolved [¹H,¹H]-NOESY, and further extended to the side-chains using 3D HBHA(CO)NH, 3D ¹³C(aliphatic)-resolved, and 3D ¹³C(aromatic)-resolved [¹H,¹H]-NOESY experiments. NOESY spectra were recorded with a mixing time of 225 ms at 800 MHz. C α , C β , H α , and N chemical shifts were used in the program TALOS²⁷ to obtain backbone torsion angles.

Structure Calculation. The software UNIO-ATNOS/CANDID^{28,29} was used in combination with the torsion angle dynamics algorithm CYANA3.0³⁰ in a standard seven-cycle protocol for NOESY peak picking, NOE assignment and structure calculation.³¹ The intensities from the NOEs were converted into distance restraints and combined with the backbone dihedral angles derived from TALOS,²⁷ of which 18 φ and ψ dihedral angle constraints predicted with high confidence were used to supplement the NOE distance restraints in the final input for structure calculations. The 40 conformers with the lowest CYANA target function values obtained from the final UNIO-ATNOS/CANDID/CYANA3.0 cycle were subjected to restrained simulated annealing and energy minimization in a water shell with the program OPALp.³² Finally, a family of 20 conformers with the lowest target function values was chosen for further analysis based on stereochemistry and energy considerations using the programs PROCHECK³³ and MOLMOL³⁴ as previously described.³¹ The structures were displayed and analyzed using PyMOL and MOLMOL.³⁴

¹⁵N Relaxation Studies. Backbone {¹H}-¹⁵N heteronuclear NOE and ¹⁵N longitudinal (T_1) and transverse (T_2) relaxation experiments were performed using standard

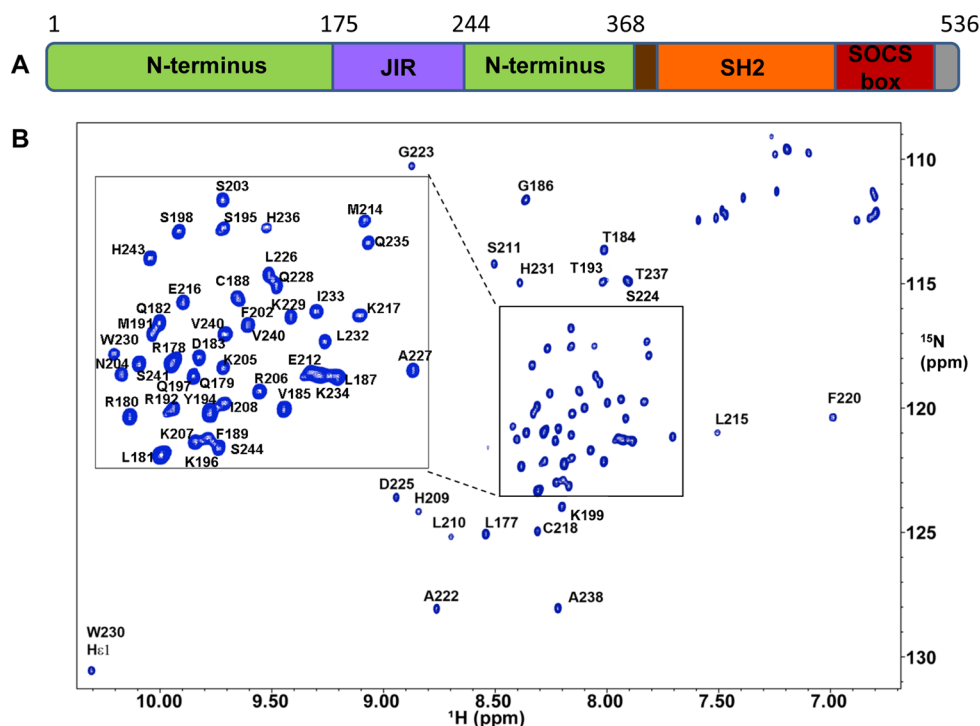


Figure 1. NMR assignments of mSOCSS_{175–244}. (A) Schematic showing domain organization in SOCSS. (B) ¹H–¹⁵N HSQC NMR spectrum of mSOCSS_{175–244} with backbone resonance assignments labeled. The spectrum was recorded in 20 mM citrate buffer, pH 4.5, containing 5 mM TCEP at 30 °C on a 600 MHz spectrometer.

methods³⁵ at 30 °C on Bruker 600 and 800 MHz spectrometers, respectively. T_1 values were obtained from a series of ¹H–¹⁵N correlation spectra with 0, 100, 400, 500, 800, 1000, 1500, and 2500 ms relaxation delays. T_2 values were acquired with 10, 30, 50, 70, 90, 110, 130, 150, 170, 190, and 210 ms delays. Recycle delay was set to 4 s for both T_1 and T_2 measurements. The relaxation rates were calculated in SPARKY by least-squares fitting of peak intensities versus relaxation delay times to an equation for single-order exponential decay. Steady-state {¹H}–¹⁵N-NOE values were determined from the ratio of peak intensities for spectra collected with and without 5 s proton presaturation.

Surface Plasmon Resonance (SPR). Surface plasmon resonance measurements were performed on a BIAcore T200 instrument at 25 °C as described previously.²² Recombinant SOCSS_{110–313} was diluted to 10 µg/mL in 10 mM sodium acetate, pH 5.0, and immobilized to a CMS Biosensor chip (GE Healthcare) using amine coupling. A reference flow cell was prepared by a similar procedure, but in the absence of protein. Recombinant JAK1 and JAK2 kinase domains were injected over the immobilized surface at a rate of 30 µL/min for 2 min in running buffer (10 mM HEPES, pH 8.0, 200 mM NaCl, 3.0 mM EDTA, 0.05% v/v Tween20) at concentrations ranging from 31.25 nM to 1 µM. Regeneration of the surface was achieved with 20 mM NaOH injected at a rate of 20 µL/min for 20s. The ligand flow cell responses were double reference subtracted for all analyses. The binding responses at the steady-state region of the sensorgrams were plotted as a function of the analyte concentration to obtain the binding curves. These curves were fitted to a steady-state model to derive the apparent equilibrium dissociation constant (K_D). Similarly, the binding affinities of mSOCSS_{175–244} and Ser211 mutants for JAK1 kinase domain were analyzed by SPR by immobilizing JAK1 kinase domain to a CMS chip using amine coupling.

Cell Transfections, Lysis, and Tryptic Digest. Flag-tagged SOCSS was transiently transfected into 293T cells using FuGENE6 (Promega), and cells were lysed 48 h later for 30 min in 1% NP-40 buffer (1% v/v NP-40, 50 mM HEPES, pH 7.4, 150 mM NaCl, 1 mM EDTA, 1 mM NaF, 1 mM Na₃VO₄). Lysates were precleared with protein-A-Sepharose prior to immunoprecipitation of Flag-tagged SOCSS with anti-Flag M2 affinity gel (Sigma). Proteins were eluted from the M2 Sepharose with 0.16% phosphoric acid (pH 1.8) on ice. Proteins were prepared for mass spectrometry analysis using the FASP protein digestion kit (Protein Discovery, Knoxville, TN) as described previously³⁶ with the following modifications: eluted material was neutralized with urea/Tris-HCl, pH 8.5 and reduced with TCEP (5 mM final concentration); 2 µg of sequence-grade modified trypsin (Promega) was added in 50 mM NH₄HCO₃ and incubated overnight at 37 °C; peptides were eluted by two rounds of washing with 40 µL of 50 mM NH₄HCO₃.

Phosphopeptide Enrichment. Tryptic peptides were subjected to phosphopeptide enrichment using the immobilized metal ion affinity chromatography (IMAC) Phosphopeptide Isolation Kit (gallium/IDA, Pierce) as per manufacturer's instructions with the following described modifications: an equal amount of binding buffer (5% acetic acid) and peptide sample was added to the resin and incubated at room temperature for 30 min. Samples were centrifuged at 1000g for 1 min and subsequently washed with 50 µL of 0.1% acetic acid followed by 50 µL of 0.1% acetic acid, 20% acetonitrile, pH 3.0. Phosphopeptides were eluted with 30 µL of 0.4 M NH₄HCO₃, 20% acetonitrile, pH 8.7 by centrifugation after incubating at room temperature for 7 min. This step was repeated twice. Phosphopeptides were acidified with formic acid (1% final concentration), subjected to vacuum centrifugation and resuspended in 25 µL 1% formic acid/2% acetonitrile.

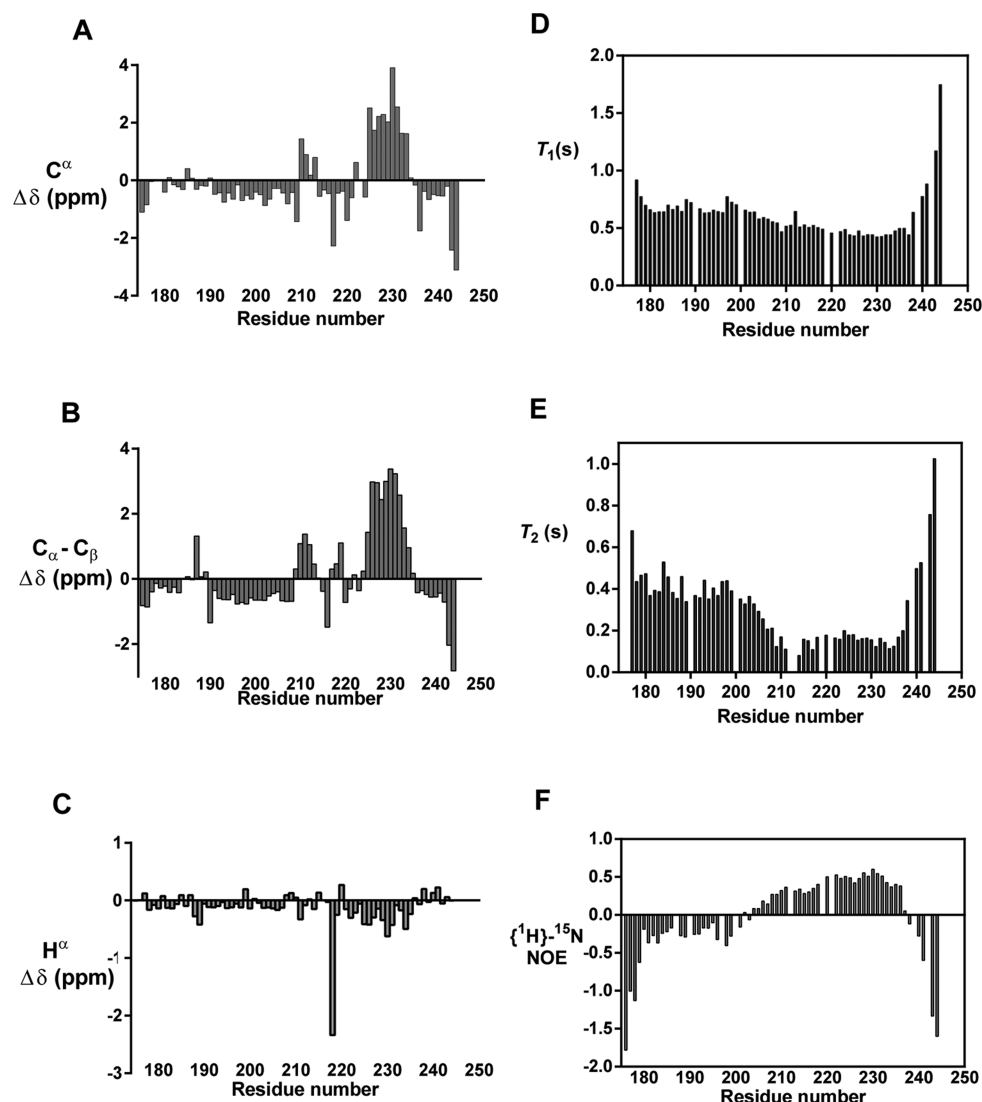


Figure 2. Secondary structure and backbone amide relaxation parameters measured for mSOCSS_{175–244}. Chemical shift deviations of (A) C α , (B) C α –C β (average over three residues), and (C) H α chemical shifts of mSOCSS_{175–244} from random-coil values are plotted vs residue number. (D–F) ^{15}N T_1 , T_2 relaxation parameters were measured at 800 MHz and steady-state $\{^1\text{H}\}$ – ^{15}N -NOE was measured at 600 MHz at 30 °C. Missing histogram bars correspond to overlapped residues and prolines.

Mass Spectrometry. Tryptic peptides were separated by nanoflow reversed-phase LC on a Waters nanoAcquity C18 150 mm \times 75 μm ID column with a 60 min gradient set at a flow rate of 400 nL/min from 100% buffer A (0.1% formic acid, 3% acetonitrile, 97% water) to 55% B (80% acetonitrile, 0.1% formic acid, 20% water). The nano HPLC was coupled online to a Q-Exactive mass spectrometer equipped with a nano-electrospray ion source (Thermo Fisher Scientific) for automated MS/MS. The Q-Exactive was run in a data-dependent acquisition mode with resolution set at 70K and the 10 most abundant precursor ions were dynamically chosen from the survey scan (350–1850 Th) for HCD fragmentation with the resolution set at 17.5K. Dynamic exclusion was enabled for 90 s.

Database Search and Identification of SOCS5 Post-translational Modifications. Mass spectra were processed using the MaxQuant software (version 1.4.1.2)³⁷ and searched against a concatenated database consisting of the Ludwig Institute nonredundant database (NR, September 2013) supplemented with common contaminants (including keratins,

trypsin, BSA) and the reversed-sequence version of the same database.³⁸ The search parameters were: minimum peptide length 7, peptide tolerance 4.5 ppm, mass tolerance 0.5 Da, cleavage enzyme trypsin/P, and a total of three missed cleavages were allowed. Carbamidomethyl (C) was set as a fixed modification, and oxidation (M), acetylation (Protein N-term), pyro-Glu/Gln (N-term) Phospho (ST), and Phospho (Y) were set as variable modifications. The peptide and protein false discovery rates (FDR) were set to 0.01. The maximal posterior error probability (PEP), which is the probability of each peptide to be a false hit considering identification score and peptide length, was set to 0.01. The ProteinProspector MS-Product program (<http://prospector.ucsf.edu/>) was used to calculate the theoretical masses of fragments of identified peptides for manual validation including a phosphopeptide corresponding to Ser211 of mouse SOCS5.

RESULTS

N-Terminus of SOCS5. The N-terminal region of SOCS5 accounts for a large proportion of the protein and is 368 amino

acid residues in length (Figure 1A). This region is enriched in polar and charged amino acids and relatively depleted in hydrophobic amino acids, a feature typical of intrinsically disordered proteins (IDPs).³⁹ The disorder prediction for SOCS5 N-terminus was made using the metaPrDOS web server, which integrates the results of eight different disorder prediction methods.⁴⁰ The prediction output is consistent with the SOCS5 N-terminus being largely unstructured, with the exception of a few short regions with ordered structure, one of which encompasses the conserved JIR (Figure S1 of the Supporting Information). Prediction of protein binding regions within the N-terminus of SOCS5 using the web server ANCHOR⁴¹ identified several segments that have the propensity to undergo disorder-to-order transition on binding a globular partner, including residues 183–192 and 210–220 in the JIR (Figure S1 of the Supporting Information).

NMR Assignments of mSOCS5_{175–244}. Given that the JIR of SOCS5 may contain some ordered structure, we expressed this region of mouse SOCS5 (residues 175–244) in *E. coli* in order to characterize its solution structure by NMR spectroscopy. The ¹H–¹⁵N HSQC spectrum of mSOCS5_{175–244} is characteristic of a largely disordered protein, with the amide proton shifts confined to 6.9–8.9 ppm (Figure 1B). While IDPs usually have uniformly sharp resonances, the mSOCS5_{175–244} spectra displayed a diversity of peak intensities and peak shapes, indicating conformational heterogeneity of the molecular ensemble. Unambiguous sequence-specific backbone assignments were obtained for all residues at 30 °C. Side chain assignments were obtained for most residues using 3D HBHA(CO)NH and 3D NOESY experiments. A representative strip plot from the 3D ¹⁵N-resolved [¹H, ¹H] NOESY spectrum for residues Leu215–Phe220 is shown in Figure S2A of the Supporting Information. The ¹³C^β chemical shifts of the two cysteine residues, Cys188 and Cys218, at 28.2 and 28.0 ppm respectively, suggested that these residues existed in the reduced state. All of the assigned proline residues were found to be in the *trans* conformation based on the presence of strong NOEs between H^δ and the preceding H^α (Figure S2B of the Supporting Information). A few minor peaks with intensities <10% of the major peaks were observed in the ¹H–¹⁵N HSQC, which might arise from minor conformers of the protein as a result of *cis*–*trans* isomerization of the prolines, but none of these resonances were assigned owing to their low intensity and the absence of cross peaks in the 3D spectra. The NMR assignments for mSOCS5_{175–244} have been deposited in the BioMagResBank database (accession no. 19966).

The JIR of SOCS5 Contains Secondary Structural Elements. The resonance assignments of mSOCS5_{175–244} were used to investigate the presence of secondary structure by evaluating the chemical shift deviations from random coil.^{42,43} The ¹³C^α and ¹³C^β secondary chemical shifts of mSOCS5_{175–244} (Figure 2A and B) show that the C-terminal region of the polypeptide, encompassing residues Asp225–Ile233, is helical, while most of the residues in the N-terminal region show essentially random coil ¹³C^α chemical shifts. The mean helix percentage for the residues Asp225–Ile233, calculated on the basis of ¹³C^α and ¹³C^β chemical shifts is 37%.⁴⁴ Secondary ¹H^α chemical shifts (Figure 2C) are consistent with helical structure in the C-terminal segment Asp225–Ile233. A chemical shift deviation of ~–2 ppm is observed for H^α of Cys218, which could be attributed to the ring current effects induced by the indole ring of Trp230 and the aromatic ring of Phe220. ¹³C^α chemical shift deviations ranging from 0.2 to 1.4 ppm were

observed in the region Leu210–Leu213 (Figure 2A), indicating the presence of transient structure in this region.

Backbone Dynamics of mSOCS5_{175–244}. Backbone {¹H}–¹⁵N-NOEs and ¹⁵N T₁ and T₂ relaxation times for mSOCS5_{175–244} are shown in Figure 2D–F. The observation of positive heteronuclear NOE values ranging from 0.2 to 0.6 for residues Ile208–His236 is consistent with limited mobility and restrained conformation in this region (Figure 2F). Residues Ser176–Ser203 in the N-terminal region and Ala238–Ser244 at the C-terminus, show negative heteronuclear NOE values, consistent with a high degree of flexibility and disorder (Figure 2F). Consistent with the heteronuclear NOE values, the T₂ values for residues His209–His236 are significantly lower than those for the rest of mSOCS5_{175–244} (Figure 2E). It is evident from the average heteronuclear NOE, T₁ and T₂ values (Table S1 of the Supporting Information) that mSOCS5_{175–244} is largely disordered. Nevertheless, the most structured region of mSOCS5_{175–244} encompassing residues Cys218–Ile233 exhibits restricted backbone mobility, with heteronuclear NOE values well above the average (Table S1 of the Supporting Information).

Solution Structure of mSOCS5_{175–244}. The C-terminal region of mSOCS5_{175–244} displayed several NOEs indicative of helix and turn-like structures (Figure S3 of the Supporting Information). Residues Ser224–Ile233 show d_{αN}(i, i + 3), d_{αβ}(i, i + 3) and d_{αN}(i, i + 4) NOEs typical for regular α-helices, indicating the presence of a fully formed α-helix in this region.⁴⁵ Furthermore, weak d_{αN}(i, i + 2) NOEs indicative of turn-like structures were observed for Ile208–Ser211 and Pro221–Gly223, although the local structure could not be classified as any specific type of turn.^{45,46} A continuous stretch of sequential NOEs supports an extended structure in the region Cys218–Phe220 preceding the turn at Pro221–Gly223. Weak d_{αN}(i, i + 2), d_{αβ}(i, i + 2), and d_{NN}(i, i + 2) NOEs were observed for residues Gln182–Val185, suggesting that this region has the propensity to adopt structure. It is possible that this localized conformation is further stabilized upon binding to a globular partner. Residues Arg175–Lys207 and Lys234–Ser244 were mostly disordered as assessed by both NOE and chemical shift analysis. Chemical shift deviations from random coil values of the C^α and H^α resonances, as well as the backbone relaxation parameters (Figure 2), are in agreement with the NOE data in identifying the most prominent secondary structure element in mSOCS5_{175–244} as an α-helix located at the C-terminus in the region Ser224–Ile233. Although there are a few long-range NOE connectivities among Cys218, Pro219, Phe220, Leu226, Ala227, and Trp230, mSOCS5_{175–244} lacks a stable tertiary structure. This is also supported by hydrogen–deuterium exchange NMR experiments, in which all backbone amide resonances underwent rapid exchange (data not shown), indicating high solvent accessibility.

Table 1 summarizes the long-range, medium-range, sequential, and intraresidue NOEs from the final cycle of UNIO-ATNOS/CANDID and CYANA 3.0.³⁰ The solution structure of mSOCS5_{175–244} is best described as a conformational ensemble of interconverting states. The global structure of the polypeptide was not well-defined, with the average root-mean-square deviation (RMSD) over the backbone heavy atoms (N, C^α, C^β) of the entire peptide being 11.2 Å. However, ordered local structure was apparent in the C-terminal region of the molecule (Figure S4 of the Supporting Information). The ensemble of 20 energy-minimized conformers that represent the most-populated state of mSOCS5_{175–244} is shown in Figure

Table 1. Structure Statistics for mSOCSS_{175–244}

no. of distance constraints	450
intraresidue ($i = j$)	189
sequential ($ i - j = 1$)	198
medium-range ($1 < i - j < 5$)	45
long-range ($ i - j \geq 5$)	18
dihedral constraints (Φ, Ψ)	18
final CYANA target function value (\AA^2)	0.70 ± 0.24
AMBER energies (kcal/mol)	
total energy	-1835 ± 115.5
van der Waals energy	-42 ± 13.2
electrostatic energy	-2426 ± 109.3
deviations from ideal geometry ^a	
bond (\AA)	0.007 ± 0.0002
angles (deg)	1.88 ± 0.061
average RMSD to mean coordinates (\AA)	
residues 218–233	
backbone heavy atoms (N, C $^\alpha$, C')	0.83 ± 0.27
All heavy atoms	1.46 ± 0.28
residues 224–233	
backbone heavy atoms (N, C $^\alpha$, C')	0.49 ± 0.17
All heavy atoms	1.12 ± 0.23
Ramachandran plot ^b	
residues 175–244	
most favored (%)	50.5
additionally allowed (%)	41.6
generously allowed (%)	4.6
disallowed (%)	3.3
residues 224–233	
most favored (%)	100
additionally allowed (%)	0
generously allowed (%)	0
disallowed (%)	0

^aThe values for the bond and angle show the deviations from ideal values based on perfect stereochemistry. ^bAs determined by PROCHECK-NMR for all residues except Gly and Pro.

3A. The ensemble of 20 structures showed excellent agreement with the experimental data, with RMSD values to the mean coordinates of 0.49 \AA for the backbone and 1.12 \AA for all heavy atoms in the structured region of residues Ser224–Ile233 (Figure 3B). Angular order parameters (S) were used to determine the precision of dihedral angles within the ensemble; the φ and ψ angles were generally well ordered ($S \geq 0.8$) for residues Ile208–Ser211 and Ser224–Ile233 (Figure S5 of the Supporting Information). The final conformers had no distance violations >0.2 \AA or dihedral violations $>5^\circ$. The NMR ensemble for mSOCSS_{175–244} has been deposited in the Protein Data Bank (PDB ID 2N34).

The transient local structure in mSOCSS_{175–244} could be stabilized by hydrophobic interactions involving Cys218, Pro219, Phe220, Pro221, Leu226 and Trp230 (Figure 3C). The exceptional upfield shift of the Phe220 backbone amide resonance observed in the ^1H – ^{15}N HSQC NMR spectrum could be due to the adjacent proline residues, Pro219 and Pro221. Positionally conserved prolines are present both N-terminal (Pro219 and Pro221) and C-terminal (Pro239) to the α -helix in mSOCSS_{175–244}, and their high degree of

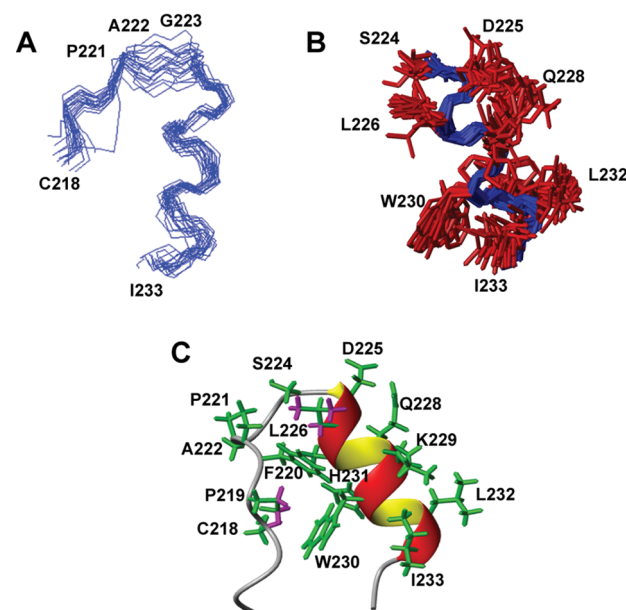


Figure 3. Solution structure of mSOCSS_{175–244}. (A) Ensemble of 20 conformers of mSOCSS_{175–244} with backbone heavy atoms superimposed over residues 218–233 (RMSD 0.83 \AA) and (B) with all heavy atoms superimposed over residues 224–233 (RMSD 1.12 \AA). (C) Closest-to-average conformer of mSOCSS_{175–244} over residues 218–233. The side chain protons of Cys218, Pro219, and Leu226 that display ring current shifts due to their proximity to the aromatic rings of Trp230 and Phe220 are highlighted in magenta. The poorly defined disordered regions of the polypeptide are not shown in the figure.

conservation suggests a positive selective pressure to maintain prolines in positions flanking this α -helix. Both Pro219 and Pro221 appear to stabilize the helix via several hydrophobic interactions. Prolines flanking prestructured elements in IDPs are thought to modulate the length and stability of these structures and therefore influence the plasticity of IDPs, which in turn dictates the functional diversity of these proteins.^{47,48}

As a consequence of the spatial proximity of Cys218, Pro219 and Leu226 to the aromatic rings of Phe220 and Trp230 (Figure 3C), some of their side chain resonances are perturbed by ring current effects. The differences between the observed and calculated average ring current shifts (Table S2 of the Supporting Information) for these resonances arise from the variability in the calculated shifts across the ensemble owing to sparse NOE restraints and less well-defined side chains of Phe220 and Trp230 (Figure S4D of the Supporting Information).

Interaction of SOCS5 N-Terminal Region with the Kinase Domain of JAK. Previously, we showed that mSOCSS_{175–244} binds specifically to the kinase domain of the JAKs with an equilibrium dissociation constant of 0.5 μM .²² Although mSOCSS_{175–244} was sufficient for binding to the JAK kinase domain, additional residues of the N-terminus were required for inhibition of JAK activity. Deletion analysis of the SOCS5 N-terminus identified a larger segment (residues 110–313) as being critical for inhibition of JAK activity.²² To determine whether this larger segment made additional contacts with the JAK kinase domain, we generated recombinant protein corresponding to mSOCSS_{110–313} and measured its binding affinity for JAK1 and JAK2 kinase domains by SPR. mSOCSS_{110–313} bound the JAK1 and JAK2 kinase domains with equilibrium dissociation constants of 0.23

and 1.5 μM , respectively (Figure 4), demonstrating that high affinity binding of mSOCSS_{175–244} to the JAK kinase domain is

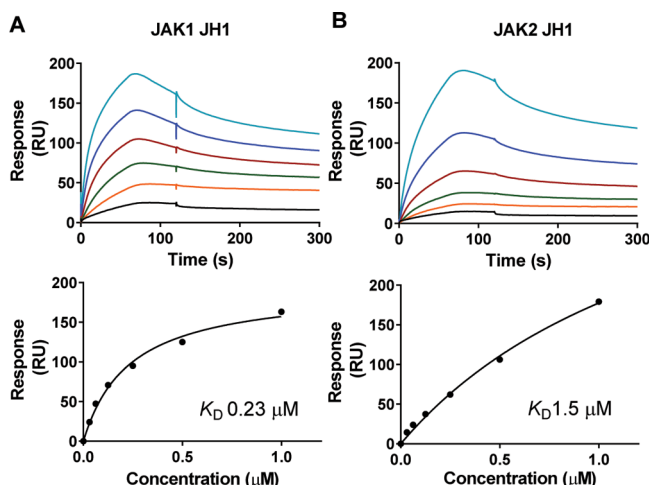


Figure 4. mSOCSS_{110–313} binds JAK kinase domain with high affinity. SPR analysis of mSOCSS_{110–313} binding to (A) JAK1 and (B) JAK2 JH1 domain. Serially diluted JAK JH1 domains (31.25 nM to 1 μM) were flowed over immobilized mSOCSS_{110–313}. Binding affinities were determined using steady-state analysis.

recapitulated by mSOCSS_{110–313} and further validating mSOCSS_{175–244} as the primary JAK interaction region in the SOCS5 N-terminus.

Identification of a Phosphorylation Site in SOCS5 JIR and its Role in JAK Binding. Post-translational modifications such as phosphorylation often regulate interactions between proteins and are known to modulate the function of intrinsically disordered proteins.^{49,50} Using mass spectrometry, we identified Ser211 within the JAK interaction region (JIR) of SOCS5, as a candidate phosphorylation site (Figure 5A). 293T cells were transiently transfected with full-length, Flag-tagged SOCS5, and the protein was enriched from cell lysates, digested with trypsin, and analyzed for the presence of phosphorylation modifications by mass spectrometry. A high confidence peptide corresponding to phosphorylated Ser211 was identified with a MaxQuant score of 143.25. Ser211 is located within a turn-like structure adjacent to the structured region (Figure 5B) in the JIR of SOCS5 and had the potential to impact on JAK binding to this region.

In order to investigate the effect of Ser211 phosphorylation on the structure and function of mSOCSS_{175–244}, Ser211 was mutated either to the phosphomimetic glutamic acid or to alanine. These mutations had no deleterious effects on either the protein expression or yield. The effect of these mutations on the structure of mSOCSS_{175–244} was analyzed by NMR spectroscopy (Figure S6 of the Supporting Information). Chemical shift changes in the 1D NMR spectra of the Ser211Glu and Ser211Ala mutants appear to be limited to the mutated residue and its adjacent residues. No significant change in chemical shift dispersion was observed in the 1D NMR spectra of the mutants, suggesting that phosphorylation of Ser211 does not induce folding or disrupt the structured region of mSOCSS_{175–244}.

Surface plasmon resonance was used to probe the role of Ser211 phosphorylation in JAK binding (Figure 6). The phosphomimetic mutant (Ser211Glu) of mSOCSS_{175–244} bound the JAK1 kinase domain with an equilibrium

dissociation constant of 0.3 μM (Figure 6B). The kinetics of Ser211Glu mutant binding to JAK1 show fast association and slow dissociation phases similar to that of the wild-type. The kinetic data could not be fit to a 1:1 binding model, thus precluding accurate quantification of the association and dissociation rates. Replacement of Ser211 with alanine resulted in a slight decrease in affinity for the JAK1 kinase domain ($K_D \sim 0.85 \mu\text{M}$) (Figure 6C). Thus, our SPR data show that mSOCSS_{175–244} and its phosphomimetic Ser211Glu mutant bind JAK1 with similar affinities, suggesting that phosphorylation of Ser211 only had a moderate effect on modulating JAK1 binding. It is also possible that phosphorylation of Ser211 modulates other interactions of the JIR or plays a more important role in the context of the full-length protein.

DISCUSSION

Intrinsically disordered regions of proteins play specific roles in protein–protein recognition,^{51,52} but their modes of interaction with partner proteins are distinct from those used by their folded counterparts. IDPs utilize a multitude of binding processes, including folding-coupled to-binding, conformational selection and “fly casting”, and the increased flexibility in IDPs is inherent to these processes.^{53–55} The mechanism of interaction often depends on the structure of the IDP in its unbound form.⁵⁶ Preformed structural elements in IDPs can play a crucial role in molecular recognition, so their identification and characterization is an area of active investigation.^{56,57}

In this study, we define the solution structure of the conserved JAK interaction region of mouse SOCS5 (mSOCSS_{175–244}) and characterize its binding to the kinase domain of JAK1. This is the first structural study on the apparently disordered N-terminal region of SOCS proteins and provides insights into the structure and dynamics of the JAK interaction region, which is unique to SOCS4 and SOCS5. NMR studies identified preformed structural elements in mSOCSS_{175–244} including a helical segment spanning residues Ser224–Ile233. NMR relaxation measurements support the presence of a transient population of secondary structural elements with restricted mobility for residues Ile208–His236. The presence of such motionally restricted structured regions in the SOCS5 N-terminus may provide a thermodynamic advantage by reducing the entropic penalty associated with coupled folding and binding.⁵⁸ Preformed structural elements, such as those present in mSOCSS_{175–244}, are likely to mediate interactions that play important roles in the regulation of signaling pathways.⁵⁶ The plasticity of the disordered SOCS5 N-terminus would enable it to function as a scaffold that can bind multiple components of the signaling pathway. The preformed hairpin structure in the SOCS5 JIR may contribute to the scaffolding functionality of the N-terminus by spatially constraining the flanking disordered regions and the proteins bound to them, thus bringing together various signaling components in close proximity to JAK, facilitating efficient interactions. On the other hand, the disordered regions flanking the SOCS5 JIR may contribute to the functional promiscuity inherent to IDPs involved in signaling pathways. It is possible that the disordered regions flanking the SOCS5 JIR retain their disordered state in the signaling complex and modulate the functions of SOCS5 through transient “fuzzy” interactions.⁵⁴ Such interactions often modulate the conformational equilibria of preformed structural elements in IDPs and aid in conformational selection.⁵⁹

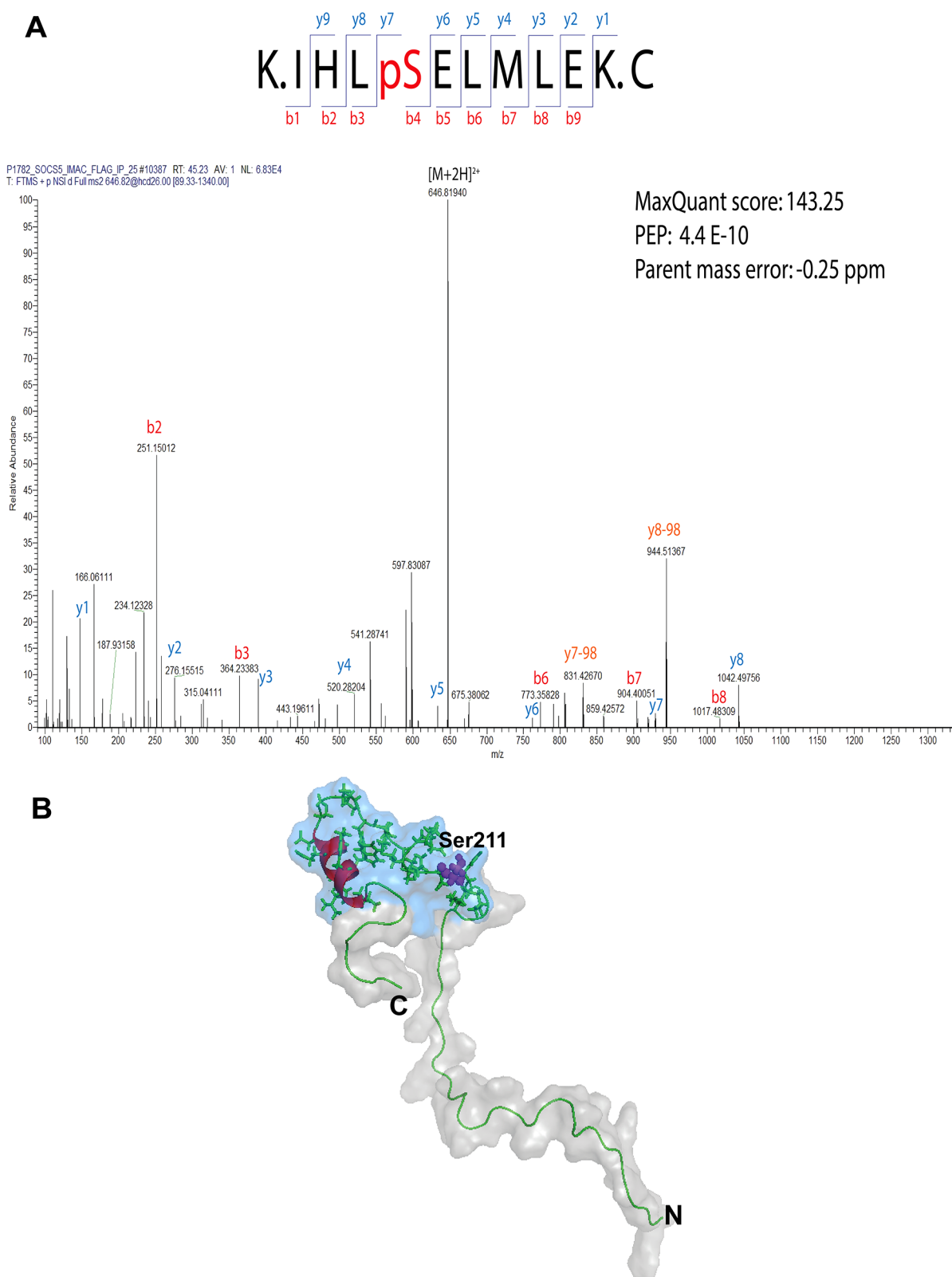


Figure 5. SOCSS JIR contains a serine phosphorylation site. (A) MS/MS spectrum identifying SOCSS phosphorylation site at Ser211. The spectrum displayed prominent product ions at 944.5 m/z and 831.4 m/z that corresponded to loss of H_3PO_4 from the y8 and y7 ions, respectively. Furthermore, the fragmentation pattern shows long uninterrupted b- and y-ion series that define the phosphopeptide sequence and site of phosphorylation. (B) Surface representation of the closest-to-average NMR conformer of mSOCSS_{175–244} with the phosphorylation site (Ser211) highlighted in purple. The surface is shown at 60% transparency, and the regions exhibiting restricted backbone mobility are shaded blue.

Phosphorylation is often overrepresented in disordered regions of proteins and is implicated in modulating the activity

of these regions.^{49,50,60} The identification of Ser211 as a candidate phosphorylation site on SOCSS adds weight to the

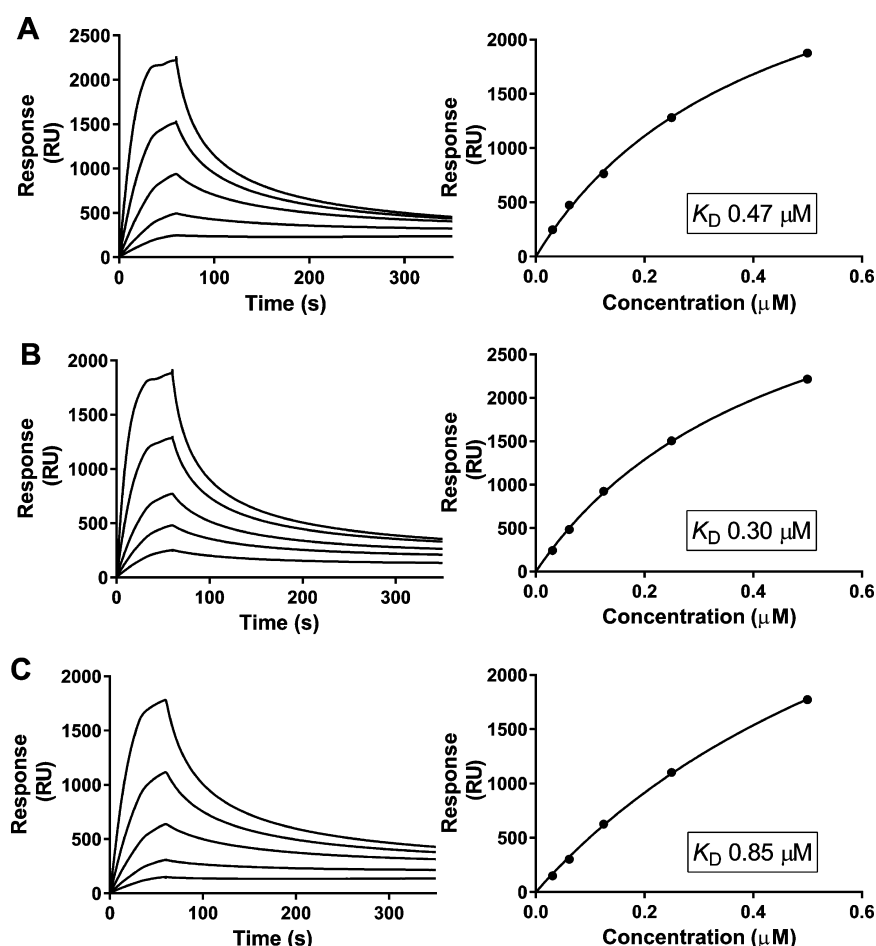


Figure 6. Effect of Ser211 phosphorylation on JAK1 binding. SPR analysis of (A) mSOCS5_{175–244}, (B) Ser211Glu mutant, and (C) Ser211Ala mutant binding to JAK1 kinase domain. Serially diluted mSOCS5_{175–244} and mutants (31.2–500 nM) were flowed over immobilized JAK1 JH1 domains. Left panels represent sensorgrams showing the kinetics of binding, and right panels show steady-state analysis. K_D values are representative of two experiments.

argument that the JIR is important for SOCS5 function, particularly given its conservation across species.⁶ As the primary JAK1 binding site on SOCS5 includes Ser211 and the surrounding residues, it is conceivable that phosphorylation of this residue in cells would modulate JAK1 binding. However, our SPR data on the phosphomimetic Ser211Glu mutant of SOCS5 showed only a moderate increase in affinity for the JAK1 kinase domain. It is possible that the Ser-to-Glu mutation has a weaker effect than phosphorylation or that the phosphate group is crucial for the functional effects of phosphorylation at Ser211. It appears that interaction of SOCS5 with the kinase domain of JAK1 is not critically regulated by a Ser211 phosphorylation switch; rather, phosphorylation of this residue may facilitate interaction with additional proteins or binding to another region of JAK outside its kinase domain.

In conclusion, we have confirmed the presence of preformed structural elements in the largely disordered N-terminus of SOCS5. We propose that the preformed helix in the SOCS5 JIR has mostly a structural role and serves as a “staple” that connects and spatially restricts the flanking flexible ligand binding regions in the unstructured N-terminus of SOCS5, thus favoring the binding process. We predict that the other SOCS family members with extended and disordered N-terminal regions, such as SOCS4, may exhibit similar modes of interaction. Further experiments will be required to validate

this hypothesis and define the binding mechanism. Given the role of SOCS5 in the inhibition of JAK1 activity and tumor suppression, molecular insights into the specific interactions that mediate inhibition of JAK are expected to lay the groundwork for the design of novel JAK inhibitors.

■ ASSOCIATED CONTENT

● Supporting Information

Disorder prediction for the N-terminus of mouse SOCS5 made using metaPrDOS (Figure S1), representative strip plots from 3D ¹⁵N-resolved and ¹³C (aliphatic)-resolved [¹H,¹H]-NOESY spectra of mSOCS5_{175–244} (Figure S2), schematic of characteristic NOEs identified for mSOCS5_{175–244} (Figure S3), structured regions of mSOCS5_{175–244} (Figure S4), angular order parameters of the backbone dihedral angles of mSOCS5_{175–244} (Figure S5), comparison of amide region of 1D ¹H NMR spectra of mSOCS5_{175–244}, Ser211Ala and Ser211Glu mutants (Figure S6), average ¹⁵N relaxation parameters for mSOCS5 JIR (Table S1), and comparison of the observed shift differences and the calculated ring current shifts for side-chain protons of Cys218, Pro219, and Leu226 (Table S2). The Supporting Information is available free of charge on the ACS Publications website at DOI: 10.1021/acs.biochem.5b00619.

AUTHOR INFORMATION

Corresponding Authors

*E-mail: indu.chandrashekar@monash.edu. Telephone: +613 99039101.

*E-mail: ray.norton@monash.edu. Telephone: +613 99039167.

Funding

This work was supported in part by the National Health and Medical Research Council (NHMRC), Australia (Program Grant 1016647), as well as an NHMRC IRISS Grant 361646, a Cancer Council Victoria Grant 1065180 and a Victorian State Government Operational Infrastructure Scheme grant. E.M.L. was supported by an Australian Postgraduate Award. R.S.N. acknowledges fellowship support from the NHMRC. J.M.M. and J.J.B. acknowledge fellowship support from the Australian Research Council.

Notes

The authors declare no competing financial interest.

ACKNOWLEDGMENTS

We thank Dr. Ann Kwan at the NMR facility, University of Sydney for her assistance in acquiring the NMR spectra.

ABBREVIATIONS

SOCS, suppressor of cytokine signaling; JAK, Janus kinase; STAT, signal transducer and activator of transcription; EGF, epidermal growth factor; JIR, JAK interacting region; NMR, nuclear magnetic resonance; mSOCS_{175–244}, N-terminal conserved region in mouse SOCS; SH2, Src-homology 2; miR, microRNA; SPR, surface plasmon resonance; TEV, tobacco etch virus; IDP, intrinsically disordered protein; HSQC, heteronuclear single quantum coherence; NOE, nuclear Overhauser effect; TCEP, tris(2-carboxyethyl)phosphine; RMSD, root-mean-square deviation

REFERENCES

- (1) Starr, R., Willson, T. A., Viney, E. M., Murray, L. J., Rayner, J. R., Jenkins, B. J., Gonda, T. J., Alexander, W. S., Metcalf, D., Nicola, N. A., and Hilton, D. J. (1997) A family of cytokine-inducible inhibitors of signalling. *Nature* 387, 917–921.
- (2) Alexander, W. S., and Hilton, D. J. (2004) The role of suppressors of cytokine signaling (SOCS) proteins in regulation of the immune response. *Annu. Rev. Immunol.* 22, 503–529.
- (3) Endo, T. A., Masuhara, M., Yokouchi, M., Suzuki, R., Sakamoto, H., Mitsui, K., Matsumoto, A., Tanimura, S., Ohtsubo, M., Misawa, H., Miyazaki, T., Leonor, N., Taniguchi, T., Fujita, T., Kanakura, Y., Komiya, S., and Yoshimura, A. (1997) A new protein containing an SH2 domain that inhibits JAK kinases. *Nature* 387, 921–924.
- (4) Hilton, D. J., Richardson, R. T., Alexander, W. S., Viney, E. M., Willson, T. A., Sprigg, N. S., Starr, R., Nicholson, S. E., Metcalf, D., and Nicola, N. A. (1998) Twenty proteins containing a C-terminal SOCS box form five structural classes. *Proc. Natl. Acad. Sci. U. S. A.* 95, 114–119.
- (5) Linossi, E. M., Babon, J. J., Hilton, D. J., and Nicholson, S. E. (2013) Suppression of cytokine signaling: the SOCS perspective. *Cytokine Growth Factor Rev.* 24, 241–248.
- (6) Feng, Z. P., Chandrashekar, I. R., Low, A., Speed, T. P., Nicholson, S. E., and Norton, R. S. (2012) The N-terminal domains of SOCS proteins: a conserved region in the disordered N-termini of SOCS4 and 5. *Proteins: Struct., Funct., Genet.* 80, 946–957.
- (7) Bullock, A. N., Rodriguez, M. C., Debreczeni, J. E., Songyang, Z., and Knapp, S. (2007) Structure of the SOCS4-ElonginB/C complex reveals a distinct SOCS box interface and the molecular basis for SOCS-dependent EGFR degradation. *Structure* 15, 1493–1504.

- (8) Nicholson, S. E., Metcalf, D., Sprigg, N. S., Columbus, R., Walker, F., Silva, A., Cary, D., Willson, T. A., Zhang, J. G., Hilton, D. J., Alexander, W. S., and Nicola, N. A. (2005) Suppressor of cytokine signaling (SOCS)-5 is a potential negative regulator of epidermal growth factor signaling. *Proc. Natl. Acad. Sci. U. S. A.* 102, 2328–2333.
- (9) Alexander, W. S. (2002) Suppressors of cytokine signalling (SOCS) in the immune system. *Nat. Rev. Immunol.* 2, 410–416.
- (10) Kario, E., Marmor, M. D., Adamsky, K., Citri, A., Amit, I., Amariglio, N., Rechavi, G., and Yarden, Y. (2005) Suppressors of cytokine signaling 4 and 5 regulate epidermal growth factor receptor signaling. *J. Biol. Chem.* 280, 7038–7048.
- (11) Sutherland, J. M., Keightley, R. A., Nixon, B., Roman, S. D., Robker, R. L., Russell, D. L., and McLaughlin, E. A. (2012) Suppressor of cytokine signaling 4 (SOCS4): moderator of ovarian primordial follicle activation. *J. Cell. Physiol.* 227, 1188–1198.
- (12) Seki, Y., Hayashi, K., Matsumoto, A., Seki, N., Tsukada, J., Ransom, J., Naka, T., Kishimoto, T., Yoshimura, A., and Kubo, M. (2002) Expression of the suppressor of cytokine signaling-5 (SOCS5) negatively regulates IL-4-dependent STAT6 activation and Th2 differentiation. *Proc. Natl. Acad. Sci. U. S. A.* 99, 13003–13008.
- (13) Stec, W., Vidal, O., and Zeidler, M. P. (2013) *Drosophila* SOCS36E negatively regulates JAK/STAT pathway signaling via two separable mechanisms. *Mol. Biol. Cell* 24, 3000–3009.
- (14) Herranz, H., Hong, X., Hung, N. T., Voorhoeve, P. M., and Cohen, S. M. (2012) Oncogenic cooperation between SOCS family proteins and EGFR identified using a *Drosophila* epithelial transformation model. *Genes Dev.* 26, 1602–1611.
- (15) Francipane, M. G., Eterno, V., Spina, V., Bini, M., Scerrino, G., Buscemi, G., Gulotta, G., Todaro, M., Dieli, F., De Maria, R., and Stassi, G. (2009) Suppressor of cytokine signaling 3 sensitizes anaplastic thyroid cancer to standard chemotherapy. *Cancer Res.* 69, 6141–6148.
- (16) Calvisi, D. F., Ladu, S., Gorden, A., Farina, M., Lee, J. S., Conner, E. A., Schroeder, I., Factor, V. M., and Thorgeirsson, S. S. (2007) Mechanistic and prognostic significance of aberrant methylation in the molecular pathogenesis of human hepatocellular carcinoma. *J. Clin. Invest.* 117, 2713–2722.
- (17) Zhuang, G., Wu, X., Jiang, Z., Kasman, I., Yao, J., Guan, Y., Oeh, J., Modrusan, Z., Bais, C., Sampath, D., and Ferrara, N. (2012) Tumour-secreted miR-9 promotes endothelial cell migration and angiogenesis by activating the JAK-STAT pathway. *EMBO J.* 31, 3513–3523.
- (18) Babon, J. J., McManus, E. J., Yao, S., DeSouza, D. P., Mielke, L. A., Sprigg, N. S., Willson, T. A., Hilton, D. J., Nicola, N. A., Baca, M., Nicholson, S. E., and Norton, R. S. (2006) The structure of SOCS3 reveals the basis of the extended SH2 domain function and identifies an unstructured insertion that regulates stability. *Mol. Cell* 22, 205–216.
- (19) Babon, J. J., Kershaw, N. J., Murphy, J. M., Varghese, L. N., Laktyushin, A., Young, S. N., Lucet, I. S., Norton, R. S., and Nicola, N. A. (2012) Suppression of cytokine signaling by SOCS3: characterization of the mode of inhibition and the basis of its specificity. *Immunity* 36, 239–250.
- (20) Babon, J. J., Sabo, J. K., Zhang, J. G., Nicola, N. A., and Norton, R. S. (2009) The SOCS box encodes a hierarchy of affinities for Cullin5: implications for ubiquitin ligase formation and cytokine signalling suppression. *J. Mol. Biol.* 387, 162–174.
- (21) Kershaw, N. J., Murphy, J. M., Liao, N. P., Varghese, L. N., Laktyushin, A., Whitlock, E. L., Lucet, I. S., Nicola, N. A., and Babon, J. J. (2013) SOCS3 binds specific receptor-JAK complexes to control cytokine signaling by direct kinase inhibition. *Nat. Struct. Mol. Biol.* 20, 469–476.
- (22) Linossi, E. M., Chandrashekar, I. R., Kolesnik, T. B., Murphy, J. M., Webb, A. I., Willson, T. A., Kedzierski, L., Bullock, A. N., Babon, J. J., Norton, R. S., Nicola, N. A., and Nicholson, S. E. (2013) Suppressor of Cytokine Signaling (SOCS) 5 utilises distinct domains for regulation of JAK1 and interaction with the adaptor protein Shc-1. *PLoS One* 8, e70536.

- (23) Orekhov, V. Y., and Jaravine, V. A. (2011) Analysis of non-uniformly sampled spectra with multi-dimensional decomposition. *Prog. Nucl. Magn. Reson. Spectrosc.* 59, 271–292.
- (24) Delaglio, F., Grzesiek, S., Vuister, G. W., Zhu, G., Pfeifer, J., and Bax, A. (1995) NMRPipe: a multidimensional spectral processing system based on UNIX pipes. *J. Biomol. NMR* 6, 277–293.
- (25) Johnson, B. A. (2004) Using NMRView to visualize and analyze the NMR spectra of macromolecules. *Methods Mol. Biol.* 278, 313–352.
- (26) Volk, J., Herrmann, T., and Wüthrich, K. (2008) Automated sequence-specific protein NMR assignment using the memetic algorithm MATCH. *J. Biomol. NMR* 41, 127–138.
- (27) Cornilescu, G., Delaglio, F., and Bax, A. (1999) Protein backbone angle restraints from searching a database for chemical shift and sequence homology. *J. Biomol. NMR* 13, 289–302.
- (28) Herrmann, T., Güntert, P., and Wüthrich, K. (2002) Protein NMR structure determination with automated NOE assignment using the new software CANDID and the torsion angle dynamics algorithm DYANA. *J. Mol. Biol.* 319, 209–227.
- (29) Herrmann, T., Güntert, P., and Wüthrich, K. (2002) Protein NMR structure determination with automated NOE-identification in the NOESY spectra using the new software ATNOS. *J. Biomol. NMR* 24, 171–189.
- (30) Güntert, P. (2003) Automated NMR protein structure calculation. *Prog. Nucl. Magn. Reson. Spectrosc.* 43, 105–125.
- (31) Serrano, P., Pedrini, B., Mohanty, B., Geralt, M., Herrmann, T., and Wüthrich, K. (2012) The J-UNIO protocol for automated protein structure determination by NMR in solution. *J. Biomol. NMR* 53, 341–354.
- (32) Luginbuhl, P., Güntert, P., Billeter, M., and Wüthrich, K. (1996) The new program OPAL for molecular dynamics simulations and energy refinements of biological macromolecules. *J. Biomol. NMR* 8, 136–146.
- (33) Laskowski, R. A., Rullmann, J. A., MacArthur, M. W., Kaptein, R., and Thornton, J. M. (1996) AQUA and PROCHECK-NMR: programs for checking the quality of protein structures solved by NMR. *J. Biomol. NMR* 8, 477–486.
- (34) Koradi, R., Billeter, M., and Wüthrich, K. (1996) MOLMOL: a program for display and analysis of macromolecular structures. *J. Mol. Graphics* 14, 51–55.
- (35) Farrow, N. A., Muhandiram, R., Singer, A. U., Pascal, S. M., Kay, C. M., Gish, G., Shoelson, S. E., Pawson, T., Forman-Kay, J. D., and Kay, L. E. (1994) Backbone dynamics of a free and phosphopeptide-complexed Src homology 2 domain studied by ^{15}N NMR relaxation. *Biochemistry* 33, 5984–6003.
- (36) Wisniewski, J. R., Zougman, A., Nagaraj, N., and Mann, M. (2009) Universal sample preparation method for proteome analysis. *Nat. Methods* 6, 359–362.
- (37) Cox, J., and Mann, M. (2008) MaxQuant enables high peptide identification rates, individualized p.p.b.-range mass accuracies and proteome-wide protein quantification. *Nat. Biotechnol.* 26, 1367–1372.
- (38) Moritz, R. L., Ji, H., Schutz, F., Connolly, L. M., Kapp, E. A., Speed, T. P., and Simpson, R. J. (2004) A proteome strategy for fractionating proteins and peptides using continuous free-flow electrophoresis coupled off-line to reversed-phase high-performance liquid chromatography. *Anal. Chem.* 76, 4811–4824.
- (39) Williams, R. M., Obradovic, Z., Mathura, V., Braun, W., Garner, E. C., Young, J., Takayama, S., Brown, C. J., and Dunker, A. K. (2001) The protein non-folding problem: amino acid determinants of intrinsic order and disorder. *Pac. Symp. Biocomput.*, 89–100.
- (40) Ishida, T., and Kinoshita, K. (2008) Prediction of disordered regions in proteins based on the meta approach. *Bioinformatics* 24, 1344–1348.
- (41) Dosztanyi, Z., Meszaros, B., and Simon, I. (2009) ANCHOR: web server for predicting protein binding regions in disordered proteins. *Bioinformatics* 25, 2745–2746.
- (42) Wishart, D. S., Sykes, B. D., and Richards, F. M. (1992) The chemical shift index: a fast and simple method for the assignment of protein secondary structure through NMR spectroscopy. *Biochemistry* 31, 1647–1651.
- (43) Wishart, D. S., Bigam, C. G., Holm, A., Hodges, R. S., and Sykes, B. D. (1995) ^1H , ^{13}C and ^{15}N random coil NMR chemical shifts of the common amino acids. I. Investigations of nearest-neighbor effects. *J. Biomol. NMR* 5, 67–81.
- (44) Marsh, J. A., Singh, V. K., Jia, Z., and Forman-Kay, J. D. (2006) Sensitivity of secondary structure propensities to sequence differences between α - and γ -synuclein: implications for fibrillation. *Protein Sci.* 15, 2795–2804.
- (45) Wüthrich, K. (1986) *NMR of proteins and nucleic acids*, Wiley, New York.
- (46) Rose, G. D., Gierasch, L. M., and Smith, J. A. (1985) Turns in peptides and proteins. *Adv. Protein Chem.* 37, 1–109.
- (47) Theillet, F. X., Kalmar, L., Tompa, P., Han, K. H., Selenko, P., Dunker, A. K., Daughdrill, G. W., and Uversky, V. N. (2013) The alphabet of intrinsic disorder. I. Act like a Pro: On the abundance and roles of proline residues in intrinsically disordered proteins. *Intrinsically Disordered Proteins* 1, e24360.
- (48) Lee, C., Kalmar, L., Xue, B., Tompa, P., Daughdrill, G. W., Uversky, V. N., and Han, K. H. (2014) Contribution of proline to the pre-structuring tendency of transient helical secondary structure elements in intrinsically disordered proteins. *Biochim. Biophys. Acta, Gen. Subj.* 1840, 993–1003.
- (49) Wright, P. E., and Dyson, H. J. (2015) Intrinsically disordered proteins in cellular signalling and regulation. *Nat. Rev. Mol. Cell Biol.* 16, 18–29.
- (50) Bah, A., Vernon, R. M., Siddiqui, Z., Krzeminski, M., Muhandiram, R., Zhao, C., Sonenberg, N., Kay, L. E., and Forman-Kay, J. D. (2015) Folding of an intrinsically disordered protein by phosphorylation as a regulatory switch. *Nature* 519, 106–109.
- (51) Wright, P. E., and Dyson, H. J. (1999) Intrinsically unstructured proteins: re-assessing the protein structure-function paradigm. *J. Mol. Biol.* 293, 321–331.
- (52) Uversky, V. N., Oldfield, C. J., and Dunker, A. K. (2005) Showing your ID: intrinsic disorder as an ID for recognition, regulation and cell signaling. *J. Mol. Recognit.* 18, 343–384.
- (53) Dyson, H. J., and Wright, P. E. (2002) Coupling of folding and binding for unstructured proteins. *Curr. Opin. Struct. Biol.* 12, 54–60.
- (54) Fuxreiter, M., and Tompa, P. (2012) Fuzzy complexes: a more stochastic view of protein function. *Adv. Exp. Med. Biol.* 725, 1–14.
- (55) Wright, P. E., and Dyson, H. J. (2009) Linking folding and binding. *Curr. Opin. Struct. Biol.* 19, 31–38.
- (56) Fuxreiter, M., Simon, I., Friedrich, P., and Tompa, P. (2004) Preformed structural elements feature in partner recognition by intrinsically unstructured proteins. *J. Mol. Biol.* 338, 1015–1026.
- (57) Lee, S. H., Kim, D. H., Han, J. J., Cha, E. J., Lim, J. E., Cho, Y. J., Lee, C., and Han, K. H. (2012) Understanding pre-structured motifs (PreSMos) in intrinsically unfolded proteins. *Curr. Protein Pept Sci.* 13, 34–54.
- (58) Sivakolundu, S. G., Bashford, D., and Kriwacki, R. W. (2005) Disordered p27Kip1 exhibits intrinsic structure resembling the Cdk2/cyclin A-bound conformation. *J. Mol. Biol.* 353, 1118–1128.
- (59) Fuxreiter, M. (2012) Fuzziness: linking regulation to protein dynamics. *Mol. Biosyst.* 8, 168–177.
- (60) Iakoucheva, L. M., Radivojac, P., Brown, C. J., O'Connor, T. R., Sikes, J. G., Obradovic, Z., and Dunker, A. K. (2004) The importance of intrinsic disorder for protein phosphorylation. *Nucleic Acids Res.* 32, 1037–1049.